

 Open access • Journal Article • DOI:10.1109/TSTE.2019.2957568

## System Strength and Inertia Constrained Optimal Generator Dispatch Under High Renewable Penetration — [Source link](#)

Huajie Gu, Ruifeng Yan, Tapan Kumar Saha, Eduard Muljadi

**Institutions:** University of Queensland, Auburn University

**Published on:** 01 Oct 2020 - IEEE Transactions on Sustainable Energy (Institute of Electrical and Electronics Engineers (IEEE))

**Topics:** Electric power system and Inertia

Related papers:

- [Cooperative Virtual Inertia and Reactive Power Control of PMSG Wind Generator and Battery for Improving Transient Stability of Power System Including Renewable Energy Sources](#)
- [Transient stability augmentation of hybrid power system based on synthetic inertia control of DFIG](#)
- [Fuzzy-Logic Based Frequency Controller for Wind Farms Augmented With Energy Storage Systems](#)
- [Inertia-Free Stand-Alone Microgrid—Part II: Inertia Control for Stabilizing DC-Link Capacitor Voltage of PMSG Wind Turbine System](#)
- [Reactive power compensation of wind permanent magnet synchronous generator - part II](#)

Share this paper:    

View more about this paper here: <https://typeset.io/papers/system-strength-and-inertia-constrained-optimal-generator-1b7z979udy>

# System Strength and Inertia Constrained Optimal Generator Dispatch under High Renewable Penetration

Huajie Gu, Student Member, *IEEE*, Ruifeng Yan, Member, *IEEE* and Tapan Saha, Fellow, *IEEE*,  
Eduard Muljadi, Fellow, *IEEE*

**Abstract**—System strength and inertia inherently provided by synchronous generators (SGs) empower a power system to ride through voltage and frequency disturbances. The requirements of system strength and inertia were not enforced in the National Electricity Market (NEM) of Australia since SGs dominated the generation fleet in the past. However, the increasing wind and solar generation continuously displaces SGs and consequently reduces system strength and inertia in the NEM.

This paper proposes a formulation of system strength and inertia constrained generator dispatch to reassure NEM operational security in light of emerging high renewable penetration. A fault current iterative solver is developed to evaluate system strength, in which the current limitation and voltage control logics of inverter-based generators, and the fault current contribution from VAR compensators are properly modelled in the phasor domain. The system strength contribution factor of an SG is defined to linearize system strength constraint for unit commitment (UC). System and sub-network inertia constraints are also formulated for the UC to limit the rate of change of frequency (RoCoF) in the event of generator/interconnector trip. The proposed generator dispatch formulation can fully meet system strength and inertia requirements in the NEM.

**Index Terms**—System strength, inertia, fault level, generator dispatch, unit commitment.

## NOMENCLATURE

### A. System Strength

$V_N$	Nominal voltage
$\vec{V}$	Voltage
$\vec{V}_0$	Pre-fault voltage
$\vec{V}_{pcc}$	Voltage at the point of common coupling
$\vec{V}_{pcc0}$	Pre-fault voltage at the point of common coupling
$V_{Npcc}$	Nominal voltage at the point of common coupling
$\vec{I}$	Current
$I_N$	Nominal current
$I_{max}$	Inverter maximum current output
$I_d$	Inverter active current output
$I_q$	Inverter reactive current output
$I_{q0}$	Pre-fault inverter reactive current
$I_f$	Fault current
$I_s$	Current output of a synchronous generator (SG)
$\vec{S}$	Apparent power
$S_{sc}$	Fault level or short-circuit capacity at a bus
$P$	Active power
$P_0$	Pre-fault active power

$P_{max}$	Inverter maximum active power output
$P_{lvpl}$	Low voltage power logic of an inverter-based generator (IBG)
$Q$	Reactive power
$Q_0$	Pre-fault reactive power
$Q_{max}$	Inverter maximum reactive power output
$\delta$	Voltage angle
$\theta$	Current angle
$\alpha$	Power angle
$K_{IBG}$	Droop of the reactive current control of an IBG
$K_{SVC}$	SVC reactive power control gain
$K_s$	Scale factor of the system strength constraint
$\vec{E}$	Equivalent voltage of an SG
$\vec{X}$	Reactance of an SG
$\vec{Y}_L$	Admittance of the equivalent inductor of an SVC
$\vec{Y}_{L0}$	Pre-fault inductance of an SVC
$\vec{Y}_C$	Admittance of the equivalent capacitor of an SVC
$\vec{Y}_{SVC}$	Total admittance of an SVC
$\mathbf{I}$	Vector of injected bus currents
$\mathbf{I}_s$	Vector of current outputs from SGs
$\mathbf{I}_f$	Vector of fault currents at fault buses
$\mathbf{Y}$	Network admittance matrix
$\mathbf{Y}_f$	Vector of fault admittances
$\mathbf{V}$	Vector of bus voltages
$\mathbf{V}_s$	Vector of terminal voltages of SGs
$\mathbf{D}_{adj}$	Adjacency matrix of ideal voltage sources
$\mathbf{J}_{adj}$	Adjacency matrix of bolted faults
$\mathbf{A}$	Augmented network matrix
$\mathbf{b}$	Vector of network knowns
$\mathbf{x}$	Vector of unknown voltages and currents
$\mathbf{x}_s$	Vector of on/off binary variables of SGs and synchronous condensers
$\Delta \vec{V}_i$	Voltage difference of the $i$ th IBG/SVC between two successive iterations
$\epsilon$	Convergence tolerance
$c_{ij}$	System strength contribution factor of the $j$ th SG to the $i$ th bus
$\mathbf{C}$	Matrix of system strength contribution factors
$\mathbf{d}_{min}$	Vector of required minimum fault levels at specified buses

### B. Inertia

$H^{sys}$	System inertia in MWs
$H_{min1}^{sys}$	Minimum required inertia constrained by the minimum permissible frequency nadir
$H_{min2}^{sys}$	Minimum required inertia constrained by the maximum permissible RoCoF
$H_i$	Inertia of an SG in MWs
$h_i$	Inertia of a synchronous condenser in MWs
$f_0$	Nominal frequency of a power system in Hz
$f_{db}$	Governor dead band in Hz

Corresponding author: Ruifeng Yan.

Huajie Gu, Ruifeng Yan and Tapan Kumar Saha are with power and energy systems research group, School of Information Technology and Electrical Engineering, The University of Queensland, Brisbane St Lucia, QLD 4072, Australia (emails: h.gu@uq.edu.au, ruifeng@itee.uq.edu.au, saha@itee.uq.edu.au).

Eduard Muljadi is with Department of Electrical and Computer Engineering, Auburn University, Auburn, AL 36849 USA (email: mze0018@auburn.edu).

$f_{\text{nadir}}$	Post-contingency frequency nadir in Hz
$f_{\text{min}}$	Permitted minimum frequency in Hz
$\text{RoCoF}^{\text{inst}}$	Instantaneous RoCoF in Hz/s
$\text{RoCoF}_{\text{max}}^{\text{inst}}$	Maximum instantaneous RoCoF in Hz/s
$G^{\text{sys}}$	Aggregated ramp rate of system primary reserve
$t_{\text{db}}$	Time frequency takes to drop below governor dead band
$t_{\text{nadir}}$	Time frequency takes to reach the nadir
$t_{\text{ramp}}$	Required time period within which the dispatched amount of system primary reserve should fully ramp up to avoid an unacceptable frequency nadir
$K_{\text{LFR}}^{\text{sys}}$	Load frequency relief constant in %/Hz
$P_{\text{load}}^{\text{sys}}$	System load in MW
$P_{\text{lost}}$	Lost power following a frequency disturbance in MW
$x_i$	On/off binary variable of an SG
$y_j$	On/off binary variable of a synchronous condenser
$p_m$	Pre-contingency power output of the $m$ th SG
$p_n$	Pre-contingency power import/export of the $n$ th sub-network
$\phi^*$	Set of a type of generators in area *. ** can be SG (synchronous generators) or SS (synchronous generators with synchronous condenser operation mode) or SC (synchronous condensers) or IBG (inverter-based generators). * can be blank (entire system) or $n$ ( $n$ th sub-network)
$\varphi^{\text{SN}}$	Set of sub-networks in a power system

### C. Unit Commitment

$\mathbf{X}$	Vector of binary variables in every dispatch interval over a period of time
$\mathbf{U}$	Vector of real variables in every dispatch interval over a period of time
$F$	Cost function
$\mathbf{g}_1$	Set of equality linear constraints
$\mathbf{g}_2$	Set of inequality linear constraints

## I. INTRODUCTION

SYSTEM strength requirements were introduced into the National Electricity Market (NEM) of Australia under the National Electricity Amendment (Managing power system fault levels) Rule 2017 No. 10 [1]. The fault level rule collectively refers system strength requirements to the minimum three-phase fault levels at chosen fault level nodes within each region of the NEM [2]. The amount of available fault levels becomes a proxy for quantifying how much system strength is required to maintain a renewable rich power system in a secure operating state. Meanwhile, inertia requirements were introduced into the NEM under the National Electricity Amendment (Managing the rate of change of power system frequency) Rule 2017 No. 9 [3]. The inertia rule highlights that the minimum level of inertia should be always kept to securely operate a NEM sub-network whenever the sub-network is islanded [4]. The Australian Energy Market Commission officially added regulation rules of system strength and inertia into the National Electricity Rules (NER) of Australia in 2018 [5].

### A. Research Problem

The NEM is projected to install more than 50 GW of wind and solar generation capacity over the next 10 years [6]. Synchronous generators (SGs) powered by burning fossil fuels will inevitably be operating less and lined up for decommission. Unlike SGs, current grid-following inverter-based generators

(IBGs), designed to capture wind and solar energy, are electromagnetically decoupled from power grids and run asynchronously. As a result, IBGs provide limited system strength, and even require a minimum system strength at their connection points to remain stable in normal operation and following a contingency event [2, 7, 8]. Unlike SGs, IBGs intrinsically have no physical inertia, and are less capable of reducing fast frequency excursions [9]. Therefore, the proliferation of IBGs brings concerns of system strength and inertia shortage in the NEM.

At present, South Australia (SA), where wind generation could be higher than the demand [10], is the only state in the NEM showing the likelihood of system strength and inertia shortfall [2, 4]. However, other states in the NEM will face the same problem as the uptake of IBGs is accelerating. Low system strength may cause unsettled voltage oscillations across the network following a voltage depression, fault-induced delayed voltage recovery [11], generator fault ride-through failure [2], and protection relay maloperation [2]. “Weak” power systems with low system strength manifest weakened resilience to voltage disturbances [8].

On the other hand, low inertia can lead to a rapid rate of change of frequency (RoCoF) [4, 12, 13]. Large RoCoF over 2 Hz/s can cause the synchronization instability of SGs [14, 15], grid-following failures of IBGs [7, 16], and inadequate responses of under frequency load shedding (UFLS) [13, 15]. “Light” power systems with low inertia may face frequency control degradation, and manifest weakened resilience to frequency disturbances [8]. Therefore, system strength and inertia requirements originate from operational security concerns of voltage and frequency control [2, 4, 17].

### B. Proposed Solution

System strength and inertia are coupled as both of them can be enhanced by dispatching greater numbers of SGs [4]. Whether system strength and inertia are adequate can be regarded as a sub-problem of unit commitment (UC), since the requirements of system strength and inertia can be ultimately translated to the requirement of the minimum number of online SGs. However, the security-constrained generator dispatch for renewable dominated power systems discussed in literature mainly considers  $N-1$  generator outage and associated inertia/reserve adequacy [12, 18-22]. Therefore, this paper proposes a formulation of system strength and inertia constrained generator dispatch with the following merits:

1. Fault current iterative solver. An iterative solver based on the augmented nodal network equation is proposed to calculate fault currents in a power system dominated by IBGs, which properly models the current limitation and voltage control logic of IBGs, and the fault current contribution from VAR compensators. The proposed solver is used to calculate the fault level of a fault level node.
2. Linearization of system strength constraint. System strength constraint is nonlinear in nature and has to be linearized so that generator dispatch solvers can address system strength requirements. The system strength contribution factor (SSCF) of an SG is developed to linearize the system strength constraint for the UC.
3. Inertia constraints. Apart from the concern of system inertia inadequacy raised by  $N-1$  generator outage, sub-network inertia shortage is also addressed in the UC to limit the RoCoF in case of network separation following the trip of the interconnector(s).

System strength indicated by the three-phase fault level at a bus is determined by the number of nearby SGs and the connected network [2]. The three-phase fault level at every chosen fault level node should always be maintained above a level so that voltage sag across the network during a fault does not cause the extensive trip of any other major electrical components such as generators [2].

The three-phase fault level or short-circuit capacity of a bus is conventionally defined as the product of the magnitudes of the nominal voltage  $V_N$  and the three-phase fault current  $I_f$  at the bus [23], given as

$$S_{sc} = V_N I_f \cdot S_{base} \text{ MVA} \quad (1)$$

where  $S_{base}$  is the system base. The only unknown in (1) is  $I_f$ . System strength at a specified location can be further simplified into the available fault current. A larger fault current indicates stronger system strength.

There are two classical phasor domain methods to calculate the fault current, including the equivalent voltage source method with correction factor (IEC 60909) [24] and the superposition method with a pre-fault power flow solution [23, 25]. However, the first method assumes a “strong” grid whilst renewable dominated power systems such as SA are “weak”. The second method models a generator as an independent voltage source behind a reactance, which is not applicable to an IBG because of its current saturation and voltage control logic. Moreover, neither of these two methods model VAR compensators. Therefore, the key to fault current calculation lies in the proper modelling of the network, generators and VAR compensators.

The proposed fault current iterative solver is shown in Fig.1. Passive components (e.g., loads and network impedances) and active components (e.g., SGs and IBGs) are the inputs. A power flow calculation is performed to initialize active components’ statuses which are used to augment the nodal network equation. The iterative solver outputs the fault current at the chosen bus. With a solved fault current, the fault level of a bus is calculated using (1).

#### A. Inverter Current Saturation

Vector control regulates real and reactive power outputs of an inverter. According to the dq0 transformation, the active current  $I_d$  and reactive current  $I_q$  of an inverter are

$$\begin{cases} I_d = \frac{P}{|\vec{V}|} \leq \frac{P_{max}}{|\vec{V}|} \\ I_q = \frac{Q}{|\vec{V}|} \leq \frac{Q_{max}}{|\vec{V}|} \end{cases} \quad (2)$$

where  $\vec{V}$  is the inverter terminal line to line voltage.  $P_{max}$  and  $Q_{max}$  are the maximum active and reactive power outputs of the inverter, respectively. Active/reactive current injection is limited to the inverter nominal current  $I_N$  to protect semiconductor switches [24], which applies a current limitation to the active/reactive current as

$$\sqrt{I_d^2 + I_q^2} \leq I_N \quad (3)$$

IBGs are required to inject reactive power in case of severe voltage upsets. NER and E.ON grid code state that an IBG must have reactive current droop control [5, 26]. When the voltage at the point of common coupling (PCC) deviates more than 10% from the nominal, the reactive current from an IBG is required to increase proportionally to the voltage deviation as [5, 26, 27]

$$\frac{I_q - I_{q0}}{I_N} = K_{IBG} \frac{|\vec{V}_{pcc0}| - |\vec{V}_{pcc}|}{V_{Npcc}} \quad (4)$$

where IBG pre-fault reactive current  $I_{q0} = Q_0 / |\vec{V}_0|$ .  $Q_0$  is the pre-fault generator reactive power output.  $\vec{V}_0$  is the pre-fault generator terminal voltage.  $\vec{V}_{pcc}$ ,  $\vec{V}_{pcc0}$  and  $V_{Npcc}$  are the IBG PCC voltage, pre-fault voltage and nominal voltage, respectively.  $K_{IBG}$  is the droop of the IBG reactive current control. NER requires that  $K_{IBG} = 4$ , i.e., an increment of the reactive current equal to 4% of the nominal for each percent of voltage drop when the voltage deviation passes the dead band of 0.1 pu [5, 28].

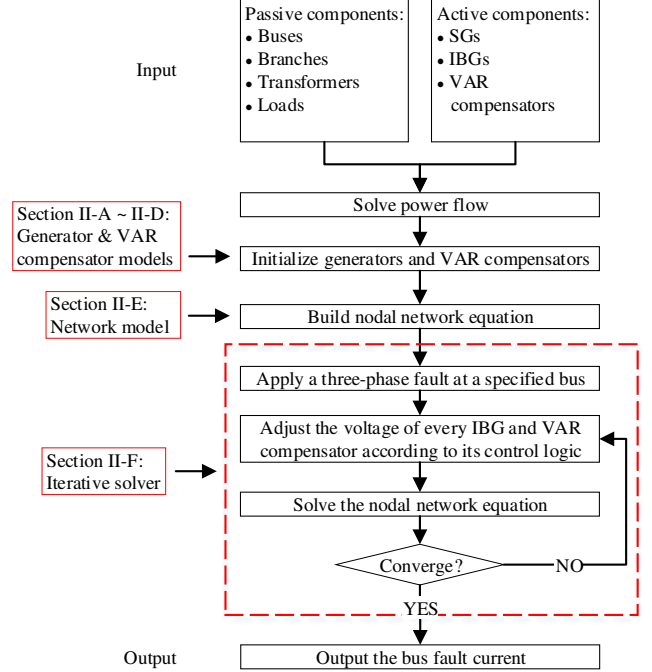


Fig. 1. Proposed fault current iterative solver.

During a low voltage period, the active power output of an IBG is restrained to give priority to reactive power injection. For instance, the low voltage power logic of General Electric (GE) 2.5 MW wind turbine is shown in Fig.2. When the terminal voltage of the wind turbine is lower than 0.9 pu, the active power output is restricted by a hard limit. The active current is then capped according to this low voltage power logic  $P_{lvpl}(|\vec{V}|)$  as

$$I_d = \frac{P_0}{|\vec{V}|} \leq \frac{P_{lvpl}(|\vec{V}|)}{V_N} \quad (5)$$

where  $P_0$  is the pre-fault generator active power output and  $V_N$  is the IBG nominal voltage.

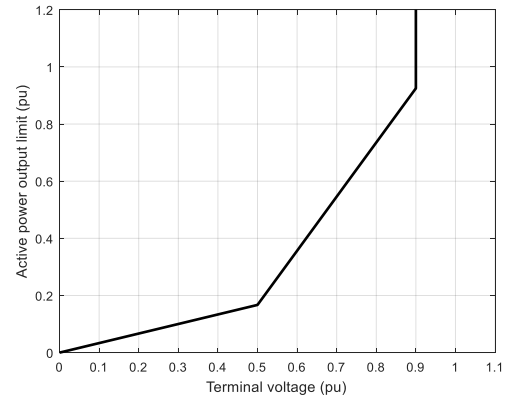


Fig. 2. GE 2.5 MW wind turbine low voltage power logic [29].

The maximum current output of an inverter is typically between 110% and 150% of the nominal [30]. Therefore, the current magnitude of the inverter during a fault is subject to

$$|\vec{I}| = \sqrt{I_d^2 + I_q^2} \leq I_{max} \quad (6)$$

## B. Inverter-based Generator Model

The saturation of inverter current output indicates that the model of a fixed voltage behind a reactance like an SG [23, 31] is not appropriate to an IBG. Instead, an IBG may be modelled as a voltage controlled current source (VCCS), as shown in Fig.3.

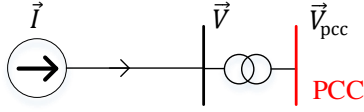


Fig. 3. Inverter-based generator model in fault analysis.

The VCCS magnitude is determined by IBG voltage control logic according to (2) ~ (6). The VCCS angle  $\theta$  can be derived from IBG active and reactive power outputs. In the abc-reference frame, the apparent power  $\vec{S}$  of an IBG is the product of the terminal voltage and the conjugate of the terminal current, given as

$$\vec{S} = \vec{V} \vec{I}^* = |\vec{V}| |\vec{I}| \angle \delta - \theta \quad (7)$$

where  $\delta$  is the terminal voltage angle. Meanwhile, in the dq0-reference frame, the voltage angle is chosen as the angle reference, so  $\vec{S}$  can also be obtained by

$$\vec{S} = P + jQ = |\vec{V}| (I_d + jI_q) = |\vec{V}| |\vec{I}| \angle \alpha \quad (8)$$

where  $\alpha$  is the power angle. Assume the phase-locked loop of the IBG successfully locks grid voltage phase, then (7) and (8) are equivalent. Substituting (8) into (7) yields the VCCS angle as

$$\theta = \delta - \alpha \quad (9)$$

## C. Synchronous Generator Model

The fault current from an SG is traditionally modelled as an independent voltage source  $\vec{E}$  behind a reactance  $\vec{X}$  [23, 31], as shown in Fig.4. The magnitude and angle of the voltage source are assumed to stay unchanged during a fault.  $\vec{E}$  can be calculated by [23]

$$\vec{E} = \vec{V}_0 + \left( \frac{P_0 + jQ_0}{\vec{V}_0} \right)^* \vec{X} \quad (10)$$

where  $\vec{X}$  can be sub-transient, transient or steady state reactance of the SG, depending on the interested timeframe.

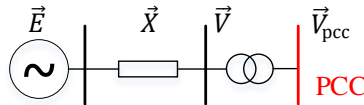


Fig. 4. Synchronous generator model in fault analysis.

## D. Static VAR Compensator Model

For an automatic admittance matching device such as a static VAR compensator (SVC), it can be modelled as a variable admittance dependent on its terminal voltage. The SVC model “CSVGN1” [32] from PSS®E is used in this paper. The simplified diagram of “CSVGN1” is shown in Fig.5. It consists of a fixed capacitor and a variable inductor. The inductor admittance  $\vec{Y}_L$  is adjusted according to the SVC terminal voltage magnitude as

$$\vec{Y}_L = \vec{Y}_{L0} + K_{svc} (|\vec{V}_0| - |\vec{V}|) \quad (11)$$

where  $\vec{Y}_{L0} = Q_0 / |\vec{V}_0|^2 - \vec{Y}_C$  is the pre-fault inductor admittance.  $\vec{Y}_C$  is the parallel capacitor admittance. An upper and lower bound should be introduced to  $\vec{Y}_L$  to respect the physical limit of the inductor. Therefore, the total admittance of the SVC is

$$\vec{Y}_{svc} = \vec{Y}_C + \vec{Y}_L \quad (12)$$

The SVC total admittance is added into network admittance matrix  $\mathbf{Y}$  to count the fault current from the SVC.

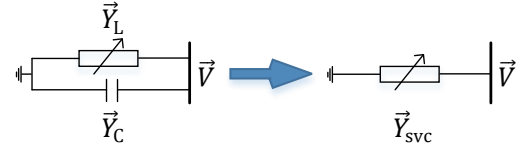


Fig. 5. Static VAR compensator (SVC) model in fault analysis.

## E. Network Model

The nodal network equation  $\mathbf{I} = \mathbf{YV}$  expressing injected bus currents in terms of bus voltages is conventionally used to estimate the voltage sag and fault currents. The nodal network equation can be augmented based on the modified augmented nodal analysis (MANA) [33]. MANA is able to introduce active components including SGs, IBGs and SVCs into nodal analysis. The augmented nodal network equation is

$$\begin{bmatrix} \mathbf{Y} & \mathbf{D}_{adj}^T & \mathbf{J}_{adj}^T \\ \mathbf{D}_{adj} & \mathbf{0} & \mathbf{0} \\ \mathbf{J}_{adj} & \mathbf{0} & \mathbf{0} \end{bmatrix} \begin{bmatrix} \mathbf{V} \\ \mathbf{I}_s \\ \mathbf{I}_f \end{bmatrix} = \begin{bmatrix} \mathbf{I} \\ \mathbf{V}_s \\ \mathbf{0} \end{bmatrix} \quad (13)$$

or

$$\mathbf{Ax} = \mathbf{b} \quad (14)$$

Loads are converted to admittances which are added into the network admittance matrix  $\mathbf{Y}$ .  $\mathbf{V}$  is the vector of unknown bus voltages.  $\mathbf{I}_s$  is the vector of unknown currents from SG equivalent voltage sources.  $\mathbf{I}_f$  is the vector of unknown fault currents at fault buses.  $\mathbf{V}_s$  is the vector of known voltages of SG equivalent voltage sources.  $\mathbf{I}$  is the vector of known bus injected currents.

An IBG is modelled as a VCCS as shown in Fig.3. The current injection of the  $i$ th bus connected with the  $j$ th IBG is  $\mathbf{I}(i) = \vec{I}_j$ .  $\vec{I}_j$  can be obtained from (4)~(9) with a known PCC voltage at present iteration. All other elements in  $\mathbf{I}$  are zero.

An SG is modelled as a constant voltage source  $\mathbf{V}_s(j)$  behind a fixed reactance as shown in Fig.4. The admittance of the SG is added into the network admittance matrix  $\mathbf{Y}$ . The voltage of the  $i$ th bus attached with the  $j$ th voltage source is known as  $\mathbf{V}(i) = \mathbf{V}_s(j)$ . Such a KVL constraint is represented by putting ‘1’ into the adjacency matrix  $\mathbf{D}_{adj}$  as  $\mathbf{D}_{adj}(j, i) = 1$ . Meanwhile, with the current of the  $j$ th voltage source injecting into the bus, the corresponding bus current injection equation becomes  $\mathbf{I}(i) = \mathbf{Y}(i, \cdot) \mathbf{V} + \mathbf{I}_s(j)$ . Such a KCL constraint is described by the transpose matrix of  $\mathbf{D}_{adj}$  as  $\mathbf{D}_{adj}^T(i, j) = 1$ . All other elements in  $\mathbf{D}_{adj}$  and  $\mathbf{D}_{adj}^T$  are zero.

## 1) Fault Analysis

For a bolted fault labeled as the  $j$ th located at the  $i$ th bus, the bus voltage is zero, i.e.,  $\mathbf{V}(i) = 0$ . Such a KVL constraint is described by putting ‘1’ into the adjacency matrix  $\mathbf{J}_{adj}$  as  $\mathbf{J}_{adj}(j, i) = 1$ . Meanwhile, with the injected fault current, the associated bus current injection equation changes to  $\mathbf{I}(i) = \mathbf{Y}(i, \cdot) \mathbf{V} + \mathbf{I}_f(j)$ . Such a KCL constraint is formulated by the transpose matrix of  $\mathbf{J}_{adj}$  as  $\mathbf{J}_{adj}^T(i, j) = 1$ . All other elements in  $\mathbf{J}_{adj}$  and  $\mathbf{J}_{adj}^T$  are zero.

For a non-bolted fault, fault bus voltage is no longer zero. Since the fault admittances  $\mathbf{Y}_f$  can be added into  $\mathbf{Y}$ ,  $\mathbf{J}_{adj}$ ,  $\mathbf{J}_{adj}^T$  and  $\mathbf{I}_f$  are removed from (13). The fault current of the  $j$ th fault branch is then calculated from a solved fault bus voltage by  $\mathbf{I}_f(j) = \mathbf{V}(i) \mathbf{Y}_f(j)$ .

## 2) Generator Trip

For an  $N-1$  SG trip event, elements associated with  $j$ th SG in  $\mathbf{Y}$ ,  $\mathbf{D}_{adj}$  and  $\mathbf{D}_{adj}^T$  are removed when formulating (13). For an  $N-1$  IBG trip event, the current injection of the  $i$ th bus connected with

the  $j$ th IBG is  $\mathbf{I}(i) = 0$ . The solution of (13) gives network voltage profile after the trip of a generator.

### 3) Multiple Contingencies

The augmented nodal network equation (13) can also investigate the voltage sag or fault currents following multiple contingencies such as multiple faults, multiple generator trips or a combination of them.

### F. Fault Current Iterative Solver

The proposed fault current iterative solver is shown in Algorithm 1. The involvement of voltage feedback control of an IBG requires an iterative adjustment of the magnitude and angle of IBG current until it does not change in the successive iterations. Similarly, the admittance of an SVC is iteratively adjusted until it does not vary any more.

The iterative process does not terminate until the difference  $\Delta|\vec{V}_i|$  between terminal voltages  $\vec{V}_i^{(m)}$  and  $\vec{V}_i^{(m-1)}$  of every IBG/SVC in two successive iterations meets the convergence tolerance  $\epsilon$ , that is

$$\Delta|\vec{V}_i| = |\vec{V}_i^{(m)} - \vec{V}_i^{(m-1)}| \leq \epsilon \quad (15)$$

where  $m$  is the  $m$ th iteration. In this paper,  $\epsilon = 10^{-4}$  pu.

#### Algorithm 1. Fault current iterative solver.

##### Step 1

Input parameters of system passive and active components (Fig.1 input).

##### Step 2

Solve power flow.

##### Step 3

Convert each load to a constant admittance evaluated at pre-fault bus voltage from power flow solution, and add the admittance into  $\mathbf{Y}$  in (13).

##### Step 4

Initialize each active component using the power flow solution. Set each SG  $\vec{X}$  and add its reciprocal into  $\mathbf{Y}$  in (13). Set each SG  $\vec{E}$  using (10) and add it into  $\mathbf{V}_s$  in (13). Set each IBG  $\vec{I}$  using (2), (3) and (7) ~ (9), and add it into  $\mathbf{I}$  in (13). Set each SVC  $\vec{V}_{svc}$  using (11) ~ (12) and add it into  $\mathbf{Y}$  in (13).

##### Step 5

Build nodal network equation (13). Set  $\mathbf{D}_{adj}$  in (13) according to bus locations of SGs. Set  $\mathbf{J}_{adj}$  in (13) according to bus locations of faults.

##### Step 6

Solve the augmented nodal network equation (13).

##### Step 7

Update each IBG  $\vec{I}$  using (4) ~ (9) according to its solved PCC voltage. Update each SVC  $\vec{V}_{svc}$  according to its solved terminal voltage using (11) and (12). Update  $\mathbf{I}$  and  $\mathbf{Y}$  in (13).

##### Step 8

Check voltage convergence using (15). Go to **Step 9** if converged, otherwise go back to **Step 6**.

##### Step 9

Output solved  $\mathbf{I}_f$  from (13).

The proposed fault current iterative solver is benchmarked against PSS@E in Appendix A. The benchmarking results demonstrate that the proposed solver provides a close estimation of three-phase fault currents in PSS@E dynamic simulations.

### G. System Strength Contribution Factor

SGs, SSs and SCs are deemed as the only system strength contributors in this paper [2]. Although the fault current from an SG can be around 3 ~ 5 times its rated current [30], an

electrically distant SG provides limited contribution to the total fault current at a bus. Therefore, the contribution of an SG to the total fault current at a specified bus is limited by its size and location.

The network admittance matrix  $\mathbf{Y}$  is capable of modelling SGs' size and location in terms of the fault current contribution. A larger-sized SG has a bigger machine admittance added into  $\mathbf{Y}$ , which in turn suggests a greater fault current output from a larger SG. Meanwhile, the SG's electrical distance to a fault location is described by branch admittances in  $\mathbf{Y}$ .

System strength adequacy is predominantly determined by the combination of online SGs [2, 34], indicating that system strength constraint is an integer constraint in the UC. Therefore, a reasonable weighting must be assigned to each SG, so that UC solvers can decide which SG should be brought online to effectively and economically boost the fault level at a targeted bus. The estimation of short-circuit power from an SG to a fault bus, defined as SSCF in this paper, is used as the weighting to linearize the system strength constraint for the UC.

The SSCF of an SG may be estimated in a stress scenario where all other generators are zeroed in the network except the studied SG. Therefore, the SSCF of the  $j$ th SG to the  $i$ th fault bus under a given system load is defined as

$$c_{ij} = S_{sc} = V_N I_f \cdot S_{base} \text{ MVA} \quad (16)$$

where  $I_f$  is obtained from solving (13) as

$$\begin{bmatrix} \mathbf{V} \\ I_s \\ I_f \end{bmatrix} = \mathbf{A}^{-1} \begin{bmatrix} \mathbf{0} \\ V_s \\ 0 \end{bmatrix}$$

Here,  $I_s$  is the current output of the  $j$ th SG, and  $I_f$  is the fault current at the  $i$ th fault bus.

### H. System Strength Constraint for Unit Commitment

To keep the minimum fault level at a fault level node, the summation of associated SSCFs of online SGs should not be less than the required threshold. Without loss of generality, system strength constraint in a generator dispatch interval for all chosen fault level nodes with a known system load is formulated as

$$K_s \mathbf{C} \mathbf{x}_s \geq \mathbf{d}_{min} \quad (17)$$

where  $K_s$  is a scale factor to calibrate SSCFs, because the short-circuit power from an SG to a fault bus in an actual system may be slightly different from the associated SSCF.  $\mathbf{C}$  is the matrix consisting of SSCFs.  $\mathbf{x}_s$  is the vector of SG on/off binary variables.  $\mathbf{d}_{min}$  is the vector of required minimum fault levels at specified fault level nodes. Eq.(17) maps the system strength constraint into the requirement of the minimum number of online SGs, which is consistent with transfer limit advice of SA system strength proposed by the Australian Energy Market Operator (AEMO) [34].

$K_s$  is a network dependent parameter that can be iteratively estimated by multiple tests of the proposed system strength constrained generator dispatch. Obviously, reducing the value of  $K_s$  can lead to more online SGs and increased fault levels. The iterative calculation of the scale factor  $K_s$  is shown in Algorithm 2. An example of  $K_s$  calculation is given in Section V-B-1.

#### Algorithm 2. Iterative calculation of the scale factor $K_s$ .

##### Step 1

Start with  $K_s = 1$ .

##### Step 2

Solve the generator dispatch problem over a period of time with the system strength constraint (17).

##### Step 3

Calculate the fault level of each fault level node in every

**Step 4**

Check whether each fault level node has adequate fault level in every dispatch interval. If not, reduce  $K_s$  by a small step (e.g., 0.1) and go back to **Step 2**, otherwise, go to **Step 5**.

**Step 5**

Output the final  $K_s$ .

### III. INERTIA

Similar to system strength, the inertia of a power system should also be maintained above a level that the post-contingency RoCoF and frequency nadir stay within permissible ranges [12].

#### A. Frequency Nadir

According to Appendix B-2, the frequency nadir following an  $N$ -1 generator trip contingency is

$$f_{\text{nadir}} = f_0 - f_{\text{db}} - \frac{f_0(P_{\text{lost}} - K_{\text{LFR}}^{\text{sys}} P_{\text{load}}^{\text{sys}} f_{\text{db}})(2P_{\text{lost}} - K_{\text{LFR}}^{\text{sys}} P_{\text{load}}^{\text{sys}} f_{\text{db}})}{8G^{\text{sys}} H^{\text{sys}} + K_{\text{LFR}}^{\text{sys}} P_{\text{load}}^{\text{sys}} f_0 (2P_{\text{lost}} - K_{\text{LFR}}^{\text{sys}} P_{\text{load}}^{\text{sys}} f_{\text{db}})} \quad (18)$$

where  $f_0$  is the nominal frequency in Hz (e.g., 50 Hz in the NEM),  $f_{\text{db}}$  is the average governor dead band (absolute value in Hz, e.g., 0.15 Hz in the NEM [35]),  $P_{\text{lost}}$  is the lost power (in MW) of the tripped generator, i.e., contingency size,  $K_{\text{LFR}}^{\text{sys}}$  is the system load frequency relief (LFR) constant in %/Hz,  $P_{\text{load}}^{\text{sys}}$  is the system load in MW,  $G^{\text{sys}}$  is the aggregated ramp rate of system primary reserve and  $H^{\text{sys}}$  is the system inertia in MWs.

Post-contingency frequency should be kept above the permitted minimum  $f_{\text{min}}$  to meet frequency operating standards (e.g., 49.5 Hz in the NEM mainland [35]). According to (18), the frequency nadir can be lifted by increasing system inertia  $H^{\text{sys}}$  or the ramp rate of system primary reserve  $G^{\text{sys}}$ .

If  $G^{\text{sys}}$  is certain, the required minimum amount of inertia  $H_{\text{min1}}^{\text{sys}}$  to maintain  $f_{\text{nadir}}$  above  $f_{\text{min}}$  is

$$H_{\text{min1}}^{\text{sys}} = \frac{f_0(P_{\text{lost}} - K_{\text{LFR}}^{\text{sys}} P_{\text{load}}^{\text{sys}} (f_0 - f_{\text{min}}))(2P_{\text{lost}} - K_{\text{LFR}}^{\text{sys}} P_{\text{load}}^{\text{sys}} f_{\text{db}})}{8G^{\text{sys}} (f_0 - f_{\text{db}} - f_{\text{min}})} \quad (19)$$

#### B. RoCoF

According to Appendix B-1, the maximum absolute instantaneous RoCoF is [8, 12]

$$\text{RoCoF}_{\text{max}}^{\text{inst}} = \frac{f_0 P_{\text{lost}}}{2H^{\text{sys}}} \quad (20)$$

$\text{RoCoF}_{\text{max}}^{\text{inst}}$  following a sizable contingency is only determined by the contingency size and available system inertia. The large the system inertia, the smaller the  $\text{RoCoF}_{\text{max}}^{\text{inst}}$ .

If the permissible  $\text{RoCoF}_{\text{max}}^{\text{inst}}$  is given, the required minimum amount of inertia  $H_{\text{min2}}^{\text{sys}}$  is

$$H_{\text{min2}}^{\text{sys}} = \frac{f_0 P_{\text{lost}}}{2\text{RoCoF}_{\text{max}}^{\text{inst}}} \quad (21)$$

Eq.(21) quantifies a conservative inertia requirement that post-contingency RoCoF is rigorously restrained to be less than the largest tolerable one. Simulation results in Appendix B-3 further demonstrate that (19) and (21) provide a conservative estimation of required inertia upon which the actual  $f_{\text{nadir}}$  and RoCoF are slightly better than the allowed  $f_{\text{min}}$  and  $\text{RoCoF}_{\text{max}}^{\text{inst}}$ .

#### C. Inertia Constraints for Unit Commitment

Since the ramp rate  $G^{\text{sys}}$  of system primary reserve cannot be fully determined without knowing the commitment of SGs,  $H_{\text{min1}}^{\text{sys}}$  is less certain. The primary reserve constraint considering the ramp rates of individual SGs proposed in [22] instead is used to restrain  $f_{\text{nadir}}$  in the UC and AC optimal power flow (OPF), which also indirectly places the inertia requirement via constraining the commitment of SGs. Therefore,  $H_{\text{min2}}^{\text{sys}}$  is chosen as the minimum inertia requirement to formulate direct inertia constraints in the UC.

In addition to SGs, synchronous condensers (SCs) and SGs with synchronous condensing capability (SSs) are also included in the generation fleet to provide flexible inertia sources. SGs retrofitted with synchronous condensing clutches can be decoupled from their driving turbines and temporarily run as SCs at the expense of a small parasitic load [36]. SCs are essentially SGs generating zero power but providing short-circuit power and inertia the same as SGs. SCs also help to minimize the curtailment of wind/solar generation as they can be quickly brought online without any minimum loading requirement [37].

##### 1) System Inertia

For a generator trip event, the contingency size  $p_m$  is the pre-contingency power output of the tripped  $m$ th generator. System inertia constraints in a dispatch interval can be formulated as [12]

$$\forall m \in \phi^{\text{SG}} \cup \phi^{\text{SS}} \cup \phi^{\text{IBG}}, \quad \sum_{i \in \phi^{\text{SG}}, i \neq m} H_i x_i + \sum_{j \in \phi^{\text{SS}}, j \neq m} (H_j x_j + h_j y_j) + \sum_{k \in \phi^{\text{SC}}} h_k y_k \geq \frac{f_0 p_m}{2\text{RoCoF}_{\text{max}}^{\text{inst}}} \quad (22)$$

where  $H_i$  is the inertia of the  $i$ th SG,  $h_j$  is the inertia of the  $j$ th SC,  $x_i$  is a binary variable representing the on/off status of the  $i$ th SG, and  $y_j$  is a binary variable indicating the on/off status of the  $j$ th SC.  $\phi^{\text{SG}}$ ,  $\phi^{\text{SS}}$ ,  $\phi^{\text{SC}}$  and  $\phi^{\text{IBG}}$  are sets of SGs, SSs, SCs and IBGs in a power system, respectively.  $i \neq m$  and  $j \neq m$  mean that the inertia of the lost SG/SS is not counted in the calculation of post-contingency system inertia.

An SS runs either as a generator or as a condenser, so the on/off status of an SS in the UC should meet

$$\forall j \in \phi^{\text{SS}}, \quad 0 \leq x_j + y_j \leq 1 \quad (23)$$

##### 2) Sub-network Inertia

Network separation caused by the Heywood trip in the SA 2016 blackout brings trip concerns of other AC interconnectors in the NEM mainland [15]. The NEM inertia rule requires that the inertia of each sub-network should be maintained above a level so that the network separation following the trip of the interconnector(s) would not result in a sizable RoCoF.

For a network separation event, the contingency size  $p_n$  of the  $n$ th sub-network is the pre-event amount of active power importing or exporting via the interconnector(s). The inertia constraints of sub-networks in a dispatch interval are

$$\forall n \in \varphi^{\text{SN}}, \quad \sum_{i \in \phi_n^{\text{SG}}} H_i x_i + \sum_{j \in \phi_n^{\text{SS}}} (H_j x_j + h_j y_j) + \sum_{k \in \phi_n^{\text{SC}}} h_k y_k \geq \pm \frac{f_0 p_n}{2\text{RoCoF}_{\text{max}}^{\text{inst}}} \quad (24)$$

where  $\varphi^{\text{SN}}$  is the set of sub-networks in a power system.  $\phi_n^{\text{SG}}$ ,  $\phi_n^{\text{SS}}$  and  $\phi_n^{\text{SC}}$  are sets of SGs, SSs and SCs in the  $n$ th

sub-network, respectively. Since the direction of interconnector power flow is unknown before generator dispatch, (24) ensures that the inertia of each sub-network is always adequate to limit RoCoF in both under-frequency and over-frequency contingency events.

#### IV. GENERATOR DISPATCH FORMULATION

The system strength and inertia constrained day-ahead half-hourly UC over 24 hours can be compactly formulated as

$$\min_{\mathbf{X}, \mathbf{U}} F(\mathbf{X}, \mathbf{U}) \quad (25)$$

subject to

$$\mathbf{g}_1(\mathbf{X}, \mathbf{U}) = \mathbf{0} \quad (26)$$

$$\mathbf{g}_2(\mathbf{X}, \mathbf{U}) \leq \mathbf{0} \quad (27)$$

where  $F$  is the quadratic cost function to be minimized.  $\mathbf{X}$  is the vector of binary variables in every dispatch interval over 24 hours, e.g., the on/off status of each SG/SS/SC  $x_j$  and/or  $y_i$  in each dispatch interval.  $\mathbf{U}$  is the vector of real variables, i.e., the amount of power and reserve from each generator/storage in every dispatch interval.

$\mathbf{g}_1$  and  $\mathbf{g}_2$  are the sets of equality and inequality linear constraints in the UC, respectively. Equation (26) refers to the DC power flow equations. Inequality constraints (27) concern the adequacy of system strength (17), the sufficiency of system inertia (22) and sub-network inertia (24), and the operational limits of network components (e.g., the maximum/minimum output of a generator/storage, the power transfer limits of an interconnector and the bounds on the state of charge of an energy storage). The formulation of coupling constraints of SGs' minimum uptime/downtime via introducing auxiliary binary variables can be found in [38]. The formulation of power ramp up/down constraints of a generator over a dispatch interval under automatic generation control can be found in [39].

Gurobi [40] is used to solve the mixed-integer quadratic programming problem of the proposed UC. The real-time generator dispatch over every five minutes is solved by AC OPF using MATPOWER [41]. Once the binary unknowns (the on/off status of every SG/SS/SC) are solved in UC, AC OPF then refines the power output and required reserve from each committed generator/storage for every five-minute dispatch.

#### V. SIMULATION RESULTS

##### A. Studied Power System

The model of Southeast Australian power system (SEAPS) [42] closely representing the NEM mainland is used to validate the proposed system strength and inertia constrained generator dispatch. As shown in Fig.6, the SEAPS is further augmented with 24 SGs, 23 wind farms and one TESLA battery storage in its Area 5 (SA) and Area 3 (Victoria (VIC)), which can reflect the wind generation capability of the NEM by the end of 2018 [43]. Four SGs in Torrens Island A power plant in SA are assumed to be retrofitted with synchronous condensing clutches and can run as SCs. A projection of daily load and wind generation of the SEAPS derived from the NEM review [44] is shown in Fig.7. Overall, the augmented SEAPS has 82 SGs, 4 SSs, 23 wind farms, 1 battery storage, 5 SVCs, 217 buses and 363 branches.

Currently, SA is the only state with the risk of system strength and inertia shortage [2, 4]. Davenport, Para and Robertstown substations are chosen as fault level nodes by AEMO in SA [2], as highlighted by the red color in Fig.6. The NEM mainland has a long and less meshed network connected by three major AC

interconnectors including the Queensland to New South Wales interconnector (QNI), Victoria to New South Wales interconnector (VNI) and Victoria to South Australia interconnector, known as the Heywood interconnector [8, 45]. Therefore, apart from  $N-1$  generator outage, this paper also accommodates single, double and triple AC interconnector trip during the generator dispatch.

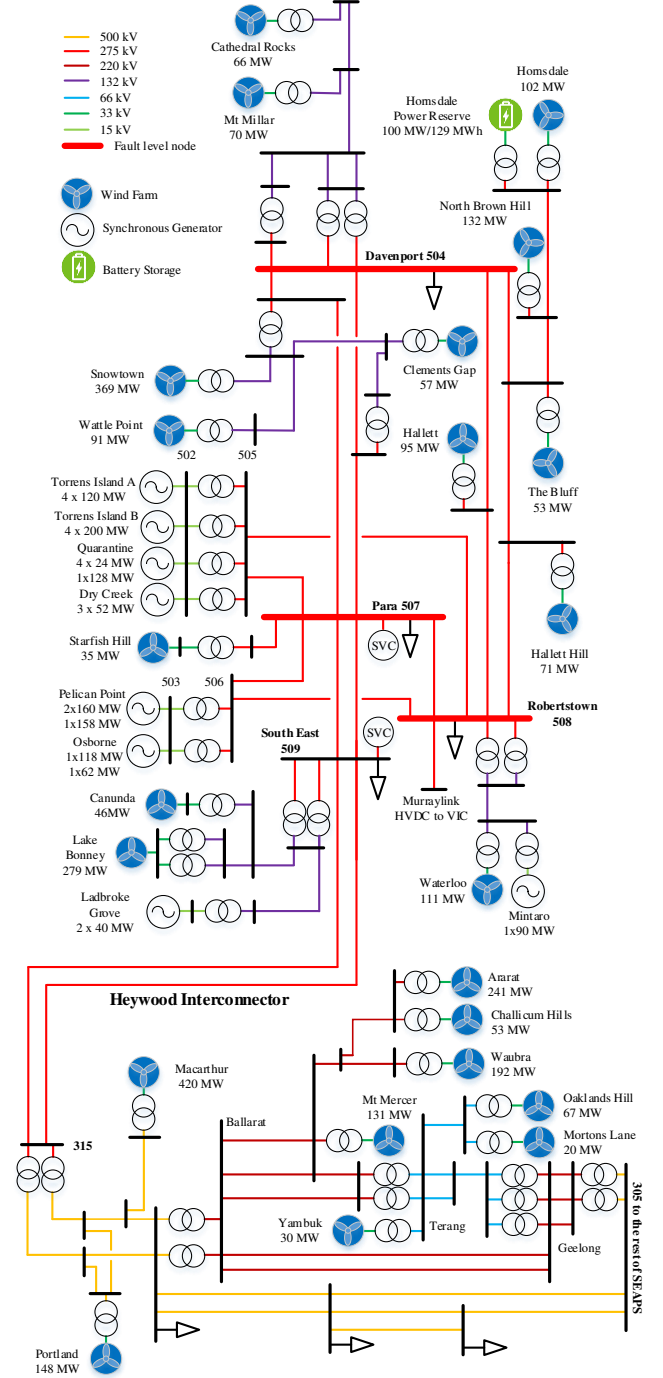


Fig. 6. South Australia and Victoria power systems [42, 43].

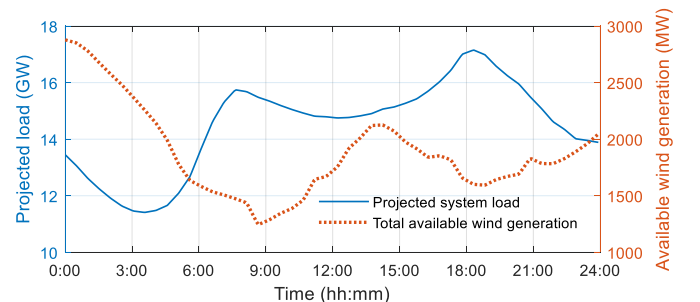


Fig. 7. A projection of daily system load and wind generation [44].

## B. System Strength

Once a real-time generator dispatch result is known from solving AC OPF, the three-phase fault level of each fault level node in SA is calculated every five minutes during the day according to Algorithm 1 and (1).

### 1) Calculation of the Scale Factor $K_s$

An example of calculating the scale factor  $K_s$  for SA system strength constraint is shown in Fig.8. As can be seen in Fig.8, when  $K_s = 1$ , the resultant fault level at Para drops below the required minimum around 12:00 and 17:00. In this example, when  $K_s$  is reduced to 0.8, Para and other two chosen fault level nodes can maintain the required fault levels throughout the day. Therefore,  $K_s = 0.8$  is chosen for SA system strength constraint in this paper.

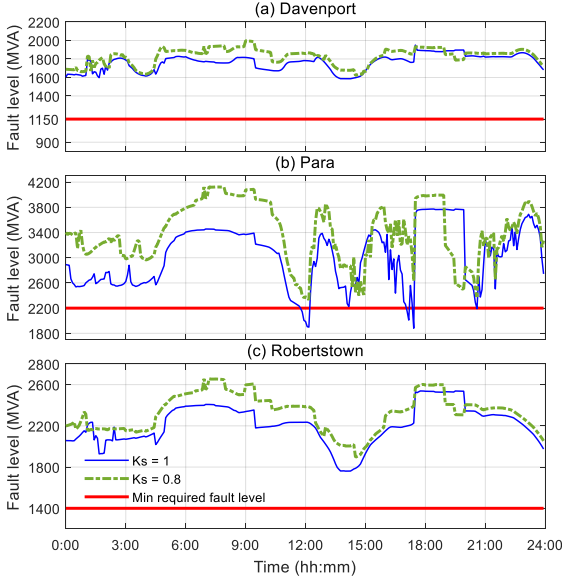


Fig. 8. An example of the iterative calculation of scale factor  $K_s$ .

### 2) Fault Levels

Fault levels at three specified fault level nodes in SA, resulted from five different generator dispatch formulations, are shown in Fig.9. The minimum required fault level of each fault level node should be maintained to warrant that SA power system can return to a stable operational state in case of the worst regional fault [2]. However, fault levels at Para, without system strength constraint (the solid blue line and solid pink line in Fig.9(b)), decline below the threshold during several hours throughout the day, particularly during the period of high wind generation.

### 3) Effectiveness of the Proposed System Strength Constraint

The placement of system strength constraint in UC can result in more SGs being dispatched, boosting the fault level of each fault level node in SA to be above the minimum required value, as indicated by the dashed orange line, dashed black line and dashed green line in Fig.9. Meanwhile, the enforcement of inertia constraints further boosts fault levels (the dashed black line against the dashed orange line in Fig.9), especially when wind power dominates the SA generation.

## C. Inertia

### 1) System Inertia

As shown in Fig.10, the inclusion of system strength and inertia constraints in UC significantly increase system inertia via dispatching more SGs during the period of high wind generation (the dashed black and green lines), in comparison to unconstrained one (the solid blue line).

### 2) Sub-network Inertia

Compared with the unconstrained generator dispatch (the

solid blue line in Fig.11(a)), inertia constraints may not always boost regional inertia or bring more SGs online (the solid pink line in Fig.11(a)), since reducing the interconnector power flow (i.e., contingency size) can also help to limit RoCoF, as shown in Fig.11(b). Consequently, inertia constraints alone cannot ensure adequate fault levels. For instance, Para still experiences an insufficient fault level with only inertia constraints, indicated by the solid pink line in Fig.9(b).

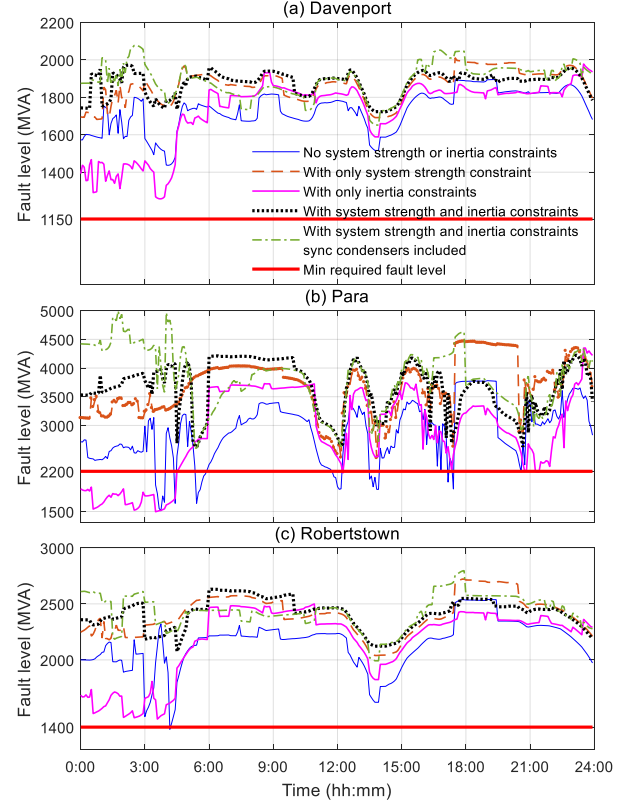


Fig. 9. Fault levels in South Australia.

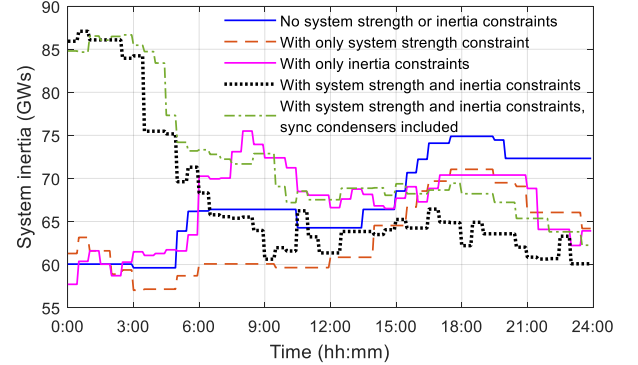


Fig. 10. System inertia of the NEM mainland (from UC result).

### 3) Effectiveness of the Proposed Inertia Constraints

Four types of contingency events (one at a time) are introduced to evaluate the effectiveness of the proposed inertia constraints. They are  $N-1$  generator outage, and single, double and triple AC interconnector trip in the NEM mainland. The largest instantaneous RoCoF in SA following each type of listed contingency events is estimated according to (A.2) for every five-minute dispatch result.

When inertia constraints are placed in generator dispatch, post-contingency RoCoF in SA can be well bounded within the permitted range of  $\pm 2$  Hz/s [14, 15], as shown in Fig.12(c), (d) and (e). It is worth noting that system strength constraint alone cannot limit RoCoF in SA, as can be seen in Fig.12(b).

## D. Wind Curtailment

Both system strength and inertia constraints should be

IEEE Transactions on Sustainable Energy enforced to ensure the adequacy of system strength and inertia. Inevitably, a large amount of wind generation in SA is curtailed during the period of high wind generation between 0:00 and 5:00 to maintain a sufficient number of online SGs, as marked by the red area in Fig.13(a).

With the operation of four SGs in Torrens Island A power station as SCs, SA wind spillage can be significantly reduced, as represented by the green area in Fig.13(a). During the period of wind peak generation, four units in Torrens Island A power station are dispatched to run as SCs (shown in Fig.13(b)). Such an operation is able to maintain the required system strength and inertia as well as to export more cheap wind power to VIC (the dashed green line against the dashed black line in Fig.11(b)).

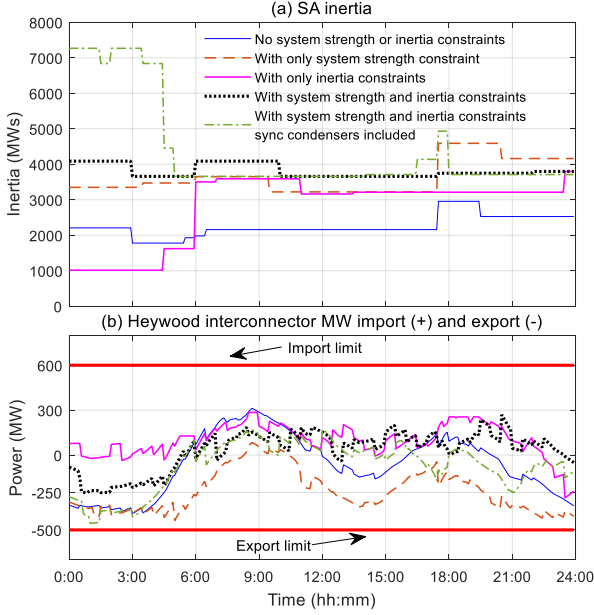


Fig. 11. Inertia in South Australia and Heywood interconnector power flow ((a) from UC result, (b) from AC OPF result).

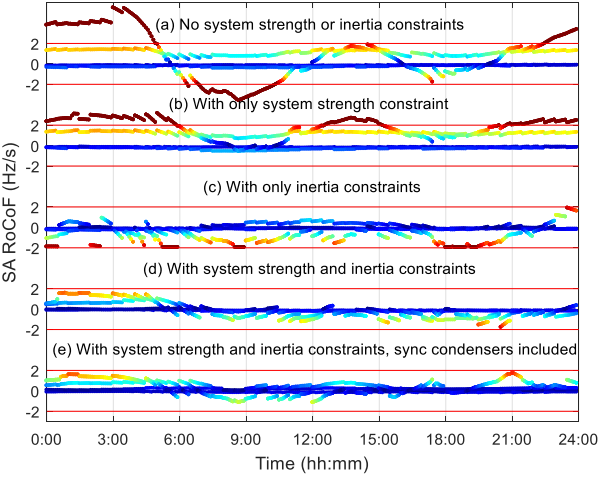


Fig. 12. Largest instantaneous RoCoF in South Australia following a frequency disturbance (estimated by Eq.(A.2) according to UC and AC OPF results).

Meanwhile, Hornsdale battery is charged to further decrease wind spillage between 0:00 and 5:00, as shown in Fig.13(c). The battery is discharged during load peaking time in the morning to sell stored wind energy, as marked by the dashed red line in Fig.13(c).

#### E. Cost Comparison

The purpose of generator dispatch is to minimize the electricity spot price under the precondition that operational security can be maintained. The SA electricity spot price is calculated every five minutes by considering SA generator outputs and the Heywood interconnector power flow solved by

AC OPF.

SA spot prices in five different cases are shown in Fig.14. The enforcement of inertia constraints alone substantially increases spot price (the solid pink line), and even causes two price spikes (the cost surge due to simultaneously bringing multiple SGs online). System strength constraint alone only mildly imposes a financial burden on SA during a high wind generation period (the dashed orange line).

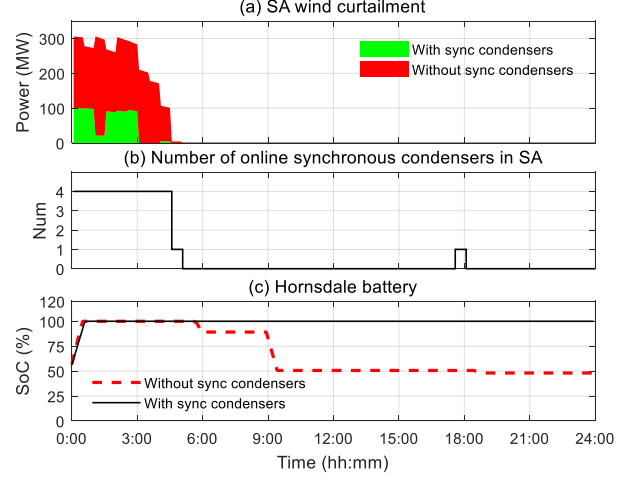


Fig. 13. Wind curtailment in South Australia and the state of change (SoC) of Hornsdale battery ((a) and (c) from AC OPF result, (b) from UC result).

SA spot price is considerably lifted with the inclusion of both system strength and inertia constraints, as shown by the dashed black line in Fig.14. However, SCs are able to reduce the spot price during the period of peak wind generation, and to retain almost the same price as if without these constraints during the rest of the day, as represented by the dashed green line in Fig.14.

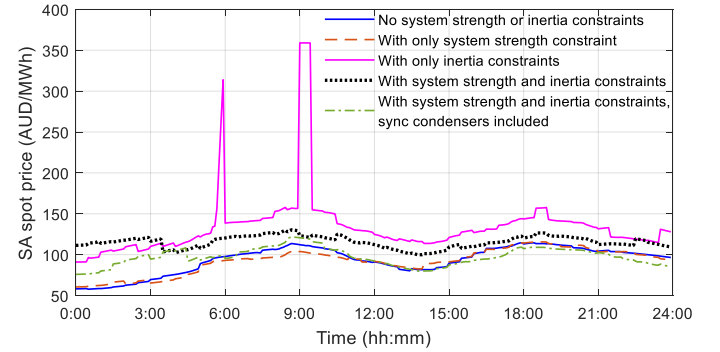


Fig. 14. Five-minute electricity spot price in South Australia.

## VI. CONCLUSION

In the near future, power systems dominated by IBGs will be operated closer to their technical boundary limits due to the reduced system strength and inertia. This paper proposed a fault current iterative solver to evaluate the system strength of a power system integrated with a large amount of IBGs, and defined the SSCF to linearize system strength constraint for the UC. The constraints of both system and sub-network inertia are also introduced to the UC to limit post-contingency RoCoF. The proposed system strength and inertia constrained generator dispatch can well satisfy the requirements of system strength and inertia under high renewable penetration.

With the proposed inertia constraints, RoCoF can be well restricted within the secure band in case of  $N-1$  generator trip or single interconnector trip or the simultaneous disconnection of multiple interconnectors. Electricity spot price goes up with the constraints of system strength and inertia, but SCs can greatly reduce spot price while providing adequate short-circuit power and inertia.

### A. Benchmarking the Proposed Fault Current Iterative Solver Against PSS@E

#### 1) IEEE 9 Bus Power System

The proposed fault current iterative solver in Section II-F is first benchmarked against PSS@E using IEEE 9 bus system in two cases, as shown in Fig.15 and TABLE I. The detailed network information can be found in [41, 46]. The inbuilt GE 2.5 MW Type-4 wind turbine model in PSS@E is used in the benchmarking [29]. The transient reactance is chosen for a SG in fault analysis, thus the PSS@E dynamic simulation results after two cycles (2c) [31] are regarded as the benchmark.

A three-phase bolted fault is applied to calculate the bus fault current. The benchmarking results listed in TABLE II and TABLE III demonstrate that the mismatches of fault currents between PSS@E dynamic simulations and the proposed solver are less than 1.5%.

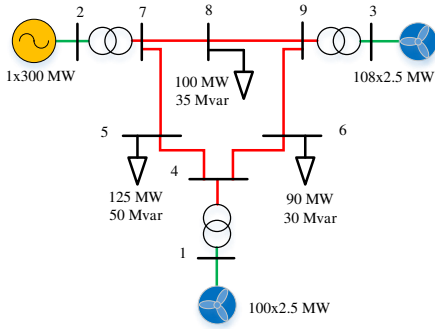


Fig. 15. IEEE 9 bus benchmark power system [41, 46].

TABLE I. CASE SETTINGS OF THE IEEE 9 BUS SYSTEM

Case	Bus 1	Bus 2	Bus 3
A	Wind	SG	SG
B	Wind	SG	Wind

TABLE II. BENCHMARKING RESULTS OF THREE-PHASE FAULT CURRENTS IN CASE A

Fault Bus No	PSS@E (2c)	Proposed solver	Error
4	6.6636 pu	6.5821 pu	1.22%
5	6.8761 pu	6.8224 pu	0.78%
6	6.6016 pu	6.5321 pu	1.05%
7	9.8260 pu	9.8165 pu	0.10%
8	8.5701 pu	8.5684 pu	0.02%
9	9.8120 pu	9.7801 pu	0.33%

TABLE III. BENCHMARKING RESULTS OF THREE-PHASE FAULT CURRENTS IN CASE B

Fault Bus No	PSS@E (2c)	Proposed solver	Error
4	6.5072 pu	6.5143 pu	0.11%
5	6.9059 pu	6.8105 pu	1.38%
6	6.1893 pu	6.14231 pu	0.76%
7	8.2648 pu	8.2594 pu	0.07%
8	7.8736 pu	7.8478 pu	0.33%
9	6.7941 pu	6.7359 pu	0.86%

#### 2) NEM Mainland Power System

The case settings of the NEM mainland power system are listed in TABLE IV. Wind penetration is defined as the percentage of wind generation over the total generation in a state (e.g., SA or VIC). Case 1 has medium wind penetration in SA and all the SGs in SA are online. Case 2 investigates the high wind penetration in SA and only four gas-powered SGs in Torrens Island power station are running. Case 3 studies the peak wind penetration at 92.6% with the operation of only one gas-powered SG in Torrens Island power station.

A three-phase bolted fault is applied to three fault level nodes

in SA (one location at a time) to calculate bus fault currents. Wind turbine dynamics in PSS@E are modelled by GE Type-3 and Type-4 wind turbine models [29]. Simulation results of Case 1 and Case 2 are shown in TABLE V and TABLE VI, respectively. The largest error between the proposed solver and PSS@E dynamic simulations is less than 4% in both cases. It further demonstrates that the proposed solver provides a close estimation of three-phase fault currents.

TABLE IV. CASE SETTINGS OF THE NEM MAINLAND POWER SYSTEM (SEAPS)

	Case 1	Case 2	Case 3
SA wind penetration level	Medium	High	Peak
SA wind penetration percentage	40.66%	69.23%	92.59%
SA Number of online SGs	20	4	1
SA wind capacity	1577 MW	1577 MW	1577 MW
SA wind generation	747 MW	900 MW	1250 MW
SA total generation	1837 MW	1300 MW	1350 MW
SA total load	2300 MW	1302 MW	1432 MW
SA power import from VIC	564 MW	43 MW	212 MW
VIC wind capacity	1302 MW	1302 MW	1302 MW
VIC wind generation	555 MW	650 MW	1000 MW
VIC total generation	5440 MW	4086 MW	4090 MW
VIC wind penetration percentage	10.20%	15.91%	24.45%
SEAPS total generation	23084 MW	14867 MW	15202 MW
SEAPS total load	22300 MW	14631 MW	14806 MW

TABLE V. BENCHMARKING RESULTS OF THREE-PHASE FAULT CURRENTS IN CASE 1

Fault Bus	PSS@E (2c)	Proposed solver	Error
Davenport	20.6116 pu	20.6773 pu	0.32%
Para	48.6559 pu	48.4445 pu	0.43%
Robertstown	25.9973 pu	25.9013 pu	0.37%

TABLE VI. BENCHMARKING RESULTS OF THREE-PHASE FAULT CURRENTS IN CASE 2

Fault Bus	PSS@E (2c)	Proposed solver	Error
Davenport	18.7872 pu	18.0618 pu	3.86%
Para	27.8988 pu	27.0035 pu	3.21%
Robertstown	24.5069 pu	23.7972 pu	2.90%

The fault currents at three fault level nodes in SA in Case 3 are listed in TABLE VII. PSS@E has consistent network convergence errors in Case 3 which only has one SG in SA. Consequently, the voltage sag propagation following a fault is widely spread in SA, which can significantly increase convergence difficulties for PSS@E. The proposed solver simplifies the network voltage calculation to the solution of a system with linear equations (13), which helps to overcome the network divergence problem of PSS@E.

TABLE VII. BENCHMARKING RESULTS OF THREE-PHASE FAULT CURRENTS IN CASE 3

Fault Bus	PSS@E (2c)	Proposed solver
Davenport	Diverge	12.4404 pu
Para	Diverge	10.7863 pu
Robertstown	Diverge	14.9735 pu

### B. Primary Frequency Control

#### 1) RoCoF

Post-contingency frequency dynamics considering LFR are conventionally modelled by the aggregated swing equation as [47]

$$\begin{aligned} \text{RoCoF}^{\text{inst}} &= \frac{df(t)}{dt} \\ &= \frac{f_0}{2H_{\text{sys}}} \left( p_{\text{mech}}(t) - p_{\text{elec}}(t) - K_{\text{LFR}}^{\text{sys}} P_{\text{load}}^{\text{sys}} (f(t) - f_0) \right) \end{aligned} \quad (\text{A.1})$$

where  $\text{RoCoF}^{\text{inst}}$  is the instantaneous RoCoF in Hz/s following

a power disturbance,  $f(t)$  is the system frequency in Hz, and  $H^{\text{sys}}$  is the system inertia in MWs.  $f_0$  is the nominal grid frequency in Hz (e.g., 50 Hz in the NEM).  $p_{\text{mech}}(t)$  and  $p_{\text{elec}}(t)$  are the total mechanical power inputs and the overall electrical power outputs of all online SGs in MW, respectively.  $K_{\text{LFR}}^{\text{sys}}$  is the system LFR constant in %/Hz.  $P_{\text{load}}^{\text{sys}}$  is the system load in MW.

It is worth noting that the LFR and governor responses reduce the instantaneous RoCoF according to (A.1). Therefore, the instantaneous RoCoF peaks at the inception of a contingency event, when governor responses are not activated and  $p_{\text{mech}}(t) - p_{\text{elec}}(t) = -P_{\text{lost}}$ . Here,  $P_{\text{lost}}$  is the lost power or contingency size in a contingency event. Therefore, the maximum absolute instantaneous RoCoF can be derived from (A.1) as [12]

$$\text{RoCoF}_{\text{max}}^{\text{inst}} = \frac{f_0 P_{\text{lost}}}{2H^{\text{sys}}} \quad (\text{A.2})$$

## 2) Frequency Nadir

The frequency nadir  $f_{\text{nadir}}$  can be estimated by calculating the definite integral of the swing equation (A.1). The integral of (A.1) between time 0 and  $t_{\text{nadir}}$  can be arranged as

$$\begin{aligned} \int_0^{t_{\text{nadir}}} \frac{df(t)}{dt} dt + \frac{K_{\text{LFR}}^{\text{sys}} P_{\text{load}}^{\text{sys}} f_0}{2H^{\text{sys}}} \int_0^{t_{\text{nadir}}} (f(t) - f_0) dt \\ = \frac{f_0}{2H^{\text{sys}}} \int_0^{t_{\text{nadir}}} (p_{\text{mech}}(t) - p_{\text{elec}}(t)) dt \end{aligned} \quad (\text{A.3})$$

The first integral on the left side of (A.3) is equal to  $f_{\text{nadir}} - f_0$ . The second integral on the left side of (A.3) may be geometrically approximated by the shaded area in the frequency deviation curve shown in Fig.16(b). Since the value of the shaded area is less than the actual integral result, such an approximation gives a conservative LFR estimation.

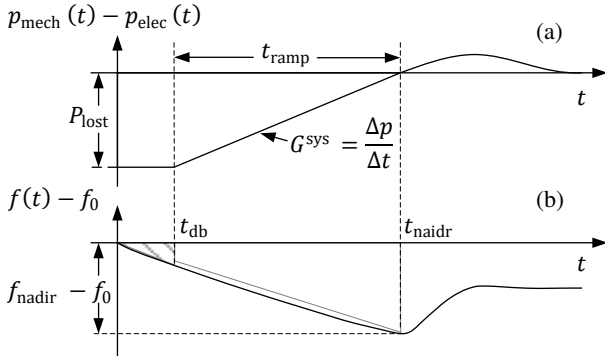


Fig. 16. Primary frequency control [22].

An aggregated ramp rate  $G^{\text{sys}}$  (in MW/s) of the overall governor responses in a power system is assumed [22] to facilitate the definite integral calculation of power imbalance on the right side of (A.3) which is equal to the shaded area in the power imbalance curve shown in Fig.16(a). Therefore, the integral result of (A.3) can be approximated by

$$\begin{aligned} f_{\text{nadir}} - f_0 + \frac{K_{\text{LFR}}^{\text{sys}} P_{\text{load}}^{\text{sys}} f_0 (f_{\text{nadir}} - f_0) t_{\text{nadir}}}{2H^{\text{sys}}} \\ = -\frac{f_0}{2H^{\text{sys}}} \left( P_{\text{lost}} t_{\text{db}} + \frac{P_{\text{lost}}^2}{2G^{\text{sys}}} \right) \end{aligned} \quad (\text{A.4})$$

where  $t_{\text{nadir}}$  is the time when the frequency reaches the nadir, given as

$$t_{\text{nadir}} = t_{\text{db}} + t_{\text{ramp}} = t_{\text{db}} + \frac{P_{\text{lost}}}{G^{\text{sys}}} \quad (\text{A.5})$$

where  $t_{\text{db}}$  is the time when the frequency drops below the

average governor dead band  $f_{\text{db}}$  (absolute value in Hz, e.g., 0.15 Hz in the NEM [35]).  $t_{\text{db}}$  can be calculated by integrating (A.1) between time 0 and  $t_{\text{db}}$  during which there are no governor responses and  $p_{\text{mech}}(t) - p_{\text{elec}}(t) = -P_{\text{lost}}$ .  $t_{\text{db}}$  is

$$t_{\text{db}} = \frac{4H^{\text{sys}} f_{\text{db}}}{f_0 (2P_{\text{lost}} - K_{\text{LFR}}^{\text{sys}} P_{\text{load}}^{\text{sys}} f_{\text{db}})} \quad (\text{A.6})$$

$t_{\text{ramp}}$  is the required time period within which the dispatched amount of system primary reserve should fully ramp up to avoid an unacceptable frequency nadir. Substituting (A.5) and (A.6) into (A.4), the post-contingency frequency nadir is

$$\begin{aligned} f_{\text{nadir}} \\ = f_0 - f_{\text{db}} - \frac{f_0 (P_{\text{lost}} - K_{\text{LFR}}^{\text{sys}} P_{\text{load}}^{\text{sys}} f_{\text{db}}) (2P_{\text{lost}} - K_{\text{LFR}}^{\text{sys}} P_{\text{load}}^{\text{sys}} f_{\text{db}})}{8G^{\text{sys}} H^{\text{sys}} + K_{\text{LFR}}^{\text{sys}} P_{\text{load}}^{\text{sys}} f_0 (2P_{\text{lost}} - K_{\text{LFR}}^{\text{sys}} P_{\text{load}}^{\text{sys}} f_{\text{db}})} \end{aligned} \quad (\text{A.7})$$

## 3) Validation of RoCoF and Frequency Nadir Estimation

A real power system (301 buses, 56 SGs, 4 IBGs and the maximum load around 1500 MW) with its actual and full dynamics in PSS@E is used to validate the derived formulas (i.e., (A.2) and (A.7)) of estimating  $\text{RoCoF}_{\text{max}}^{\text{inst}}$  and  $f_{\text{nadir}}$  following an N-1 generator trip. The test system is in an island, which is linked via an HVDC line to a large interconnected power system. The HVDC line is capable of providing fast frequency response (FFR). Frequency is allowed to reach 48 Hz in this small test system.

The case settings of the test system are shown in TABLE VIII. The primary frequency responses of the test system in two cases are shown in Fig.17. Simulation results listed in TABLE IX and TABLE X show that actual RoCoFs and frequency deviations are less than the estimated ones, proving that the proposed formulas (i.e., (A.2) and (A.7)) yield conservative results. In other words, the estimated minimum required inertia (e.g., 3500 MWs) from (19) and (21) based upon the allowed maximum RoCoF (e.g., 1 Hz/s) and the permitted minimum frequency nadir (e.g., 49.224 Hz) can guarantee the actual RoCoF and frequency deviation are less than the allowable limits, which assures the operational security of primary frequency control.

TABLE VIII. CASE SETTINGS OF THE TEST SYSTEM

	Case I	Case II
Post-contingency inertia	3500 MWs	7000 MWs
Aggregated ramp rate	95 MW/s	28 MW/s
Load	1246 MW	1246 MW
LFR constant	2 %/Hz	2 %/Hz
Nominal frequency	50 Hz	50 Hz
Frequency control dead band	0.15 Hz	0.15 Hz
HVDC line power import	300 MW	Offline
Contingency size	140 MW	140 MW

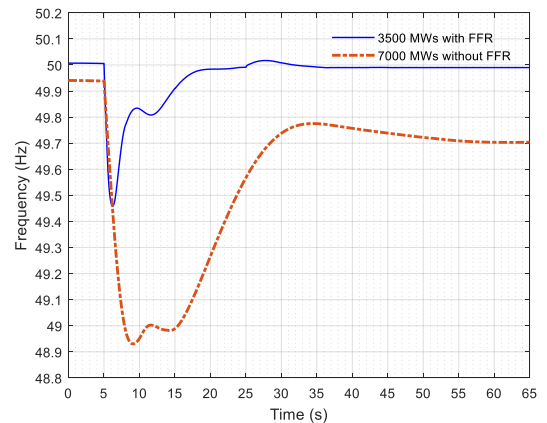


Fig. 17. Primary frequency responses of the test power system.

TABLE IX. RESULTS OF THE PRIMARY FREQUENCY RESPONSE IN CASE I

	Estimated	Actual
$\text{RoCoF}_{\max}^{\text{inst}}$	1 Hz/s	0.856 Hz/s
$f_{\text{nadir}}$	49.224 Hz	49.459 Hz

TABLE X. RESULTS OF THE PRIMARY FREQUENCY RESPONSE IN CASE II

	Estimated	Actual
$\text{RoCoF}_{\max}^{\text{inst}}$	0.5 Hz/s	0.476 Hz/s
$f_{\text{nadir}}$	48.866 Hz	48.930 Hz

#### 4) Fast Frequency Response

The response time of the FFR to a frequency disturbance is rapid, but it is generally restricted by the detection and signaling time. Adequate inertia is required to limit the initial RoCoF, buying time to facilitate robust measurement of frequency for the FFR, thus minimizing false triggering during transient frequency spikes [15]. Although the FFR from a sizable IBG (e.g., a large battery storage) increases the overall ramp rate  $G^{\text{sys}}$  of system primary reserve, it is not the key to effectively constrain  $\text{RoCoF}_{\max}^{\text{inst}}$  as discussed in Section III-B. Synthetic inertia from IBGs (e.g., emulated inertia from wind turbines) is essentially a type of the FFR [8, 15].

The benefit of the FFR is to effectively raise frequency nadir as elaborated in Section III-A. The minimum required inertia in the test power system versus the overall ramp rate of system primary reserve according to (19) is shown in Fig.18. The minimum required inertia constrained by  $\text{RoCoF}_{\max}^{\text{inst}}$  using (21) is also shown in Fig.18. All the other parameters of inertia calculation are listed in TABLE VIII.

As can be seen in Fig.18, lifting the overall ramp rate of system primary reserve by 20 MW/s in the test system with 7GWs of inertia (from A to B), the post-contingency frequency nadir can be improved by 0.36 Hz. However, a larger increment at 39 MW/s has to be added to the primary reserve to achieve the same improvement in frequency nadir if the available inertia is halved to 3.5 GWs, i.e., from D to E.

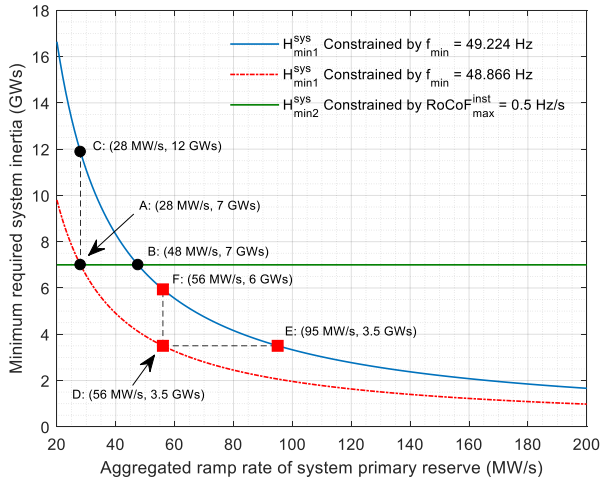


Fig. 18. Minimum required system inertia versus the ramp rate of system primary reserve in the test power system.

As illustrated in Fig.18, from A to C, 5 GWs of additional inertia is needed to improve the frequency nadir by 0.36 Hz if the ramp rate of system primary reserve is fixed at 28 MW/s. However, from D to F, less inertia is required to boost the frequency nadir by the same amount with faster primary reserve. As also shown in Fig.18, RoCoF is mainly determined by the available system inertia, no FFR can limit the maximum RoCoF to 0.5 Hz/s, if the inertia of the test system is below 7GWs.

#### REFERENCE

- [1] Australian Energy Market Commission, *National electricity amendment (managing power system fault levels) rule 2017*, 2017.
- [2] Australian Energy Market Operator. "System strength requirements methodology system strength requirements & fault level shortfalls," [https://www.aemo.com.au/-/media/Files/Electricity/NEM/Security\\_and\\_Reliability/System-Security-Market-Frameworks-Review/2018/System\\_Strength\\_Requirements\\_Methodology\\_PUBLISHED.pdf](https://www.aemo.com.au/-/media/Files/Electricity/NEM/Security_and_Reliability/System-Security-Market-Frameworks-Review/2018/System_Strength_Requirements_Methodology_PUBLISHED.pdf).
- [3] Australian Energy Market Commission, *National electricity amendment (managing the rate of change of power system frequency) rule 2017*, 2017.
- [4] Australian Energy Market Operator. "Inertia requirements methodology inertia requirements & shortfalls," [https://www.aemo.com.au/-/media/Files/Electricity/NEM/Security\\_and\\_Reliability/System-Security-Market-Frameworks-Review/2018/Inertia\\_Requirements\\_Methodology\\_PUBLISHED.pdf](https://www.aemo.com.au/-/media/Files/Electricity/NEM/Security_and_Reliability/System-Security-Market-Frameworks-Review/2018/Inertia_Requirements_Methodology_PUBLISHED.pdf).
- [5] Australian Energy Market Commission. "National Electricity Rules," <https://www.aemc.gov.au/sites/default/files/2018-12/NER%20-%20v117.pdf>.
- [6] Australian Energy Market Operator. "NEM generation information," 2019; <https://www.aemo.com.au/Electricity/National-Electricity-Market-NEM/Planning-and-forecasting/Generation-information>.
- [7] Cigre working group B4.62, *Connection of wind farms to weak AC networks*, 2016.
- [8] H. Gu, R. Yan, and T. Saha, "Review of system strength and inertia requirements for the National Electricity Market of Australia," *CSEE Journal of Power and Energy Systems*, vol. 5, no. 3, pp. 295 - 305, 2019.
- [9] Australian Energy Market Commission. "System security market frameworks review," 2019; <https://www.aemc.gov.au/sites/default/files/content/f510069a-791b-4e4d-8bc0-9e6a216be7a2/System-Security-Market-Frameworks-Review-Final-Report.pdf>.
- [10] Australian Energy Market Operator. "South Australia system strength assessment," [https://www.aemo.com.au/-/media/Files/Media\\_Centre/2017/South\\_Australia\\_System\\_Strength\\_Assessment.pdf](https://www.aemo.com.au/-/media/Files/Media_Centre/2017/South_Australia_System_Strength_Assessment.pdf).
- [11] North American Electric Reliability Corporation. "Short-circuit modeling and system strength white paper," 2019; [https://www.nerc.com/pa/RAPA/ra/Reliability%20Assessments%20DL/Short\\_Circuit\\_whitepaper\\_Final\\_1\\_26\\_18.pdf](https://www.nerc.com/pa/RAPA/ra/Reliability%20Assessments%20DL/Short_Circuit_whitepaper_Final_1_26_18.pdf).
- [12] H. Gu, R. Yan, and T. K. Saha, "Minimum synchronous inertia requirement of renewable power systems," *IEEE Transactions on Power Systems*, vol. 33, no. 2, pp. 1533 - 1543, 2018.
- [13] Australian Energy Market Operator. "Black system South Australia 28 September 2016," [https://www.aemo.com.au/-/media/Files/Electricity/NEM/Market\\_Notices\\_and\\_Events/Power\\_System\\_Incident\\_Reports/2017/Integrated-Final-Report-SA-Black-System-28-September-2016.pdf](https://www.aemo.com.au/-/media/Files/Electricity/NEM/Market_Notices_and_Events/Power_System_Incident_Reports/2017/Integrated-Final-Report-SA-Black-System-28-September-2016.pdf).
- [14] DNV KEMA Energy & Sustainability. "RoCoF an independent analysis on the ability of generators to ride through rate of change of frequency values up to 2Hz/s," [http://www.eirgridgroup.com/site-files/library/EirGrid/DNV-KEMA\\_Report\\_RoCoF\\_20130208final\\_.pdf](http://www.eirgridgroup.com/site-files/library/EirGrid/DNV-KEMA_Report_RoCoF_20130208final_.pdf).
- [15] Australian Energy Market Operator. "Fast frequency response in the NEM," [https://www.aemo.com.au/-/media/Files/Electricity/NEM/Security\\_and\\_Reliability/Reports/2017/FFR-Working-Paper---Final.pdf](https://www.aemo.com.au/-/media/Files/Electricity/NEM/Security_and_Reliability/Reports/2017/FFR-Working-Paper---Final.pdf).
- [16] R. Yan, N. A. Masood, T. K. Saha, F. Bai, and H. Gu, "The Anatomy of the 2016 South Australia Blackout: A Catastrophic Event in a High Renewable Network," *IEEE Transactions on Power Systems*, vol. 33, no. 5, pp. 5374-5388, Sep, 2018.
- [17] Australian Energy Market Operator. "Power system requirements," [https://www.aemo.com.au/-/media/Files/Electricity/NEM/Security\\_and\\_Reliability/Power-system-requirements.pdf](https://www.aemo.com.au/-/media/Files/Electricity/NEM/Security_and_Reliability/Power-system-requirements.pdf).
- [18] Y. F. Wen, W. Y. Li, G. Huang, and X. Liu, "Frequency Dynamics Constrained Unit Commitment With Battery Energy Storage," *IEEE Transactions on Power Systems*, vol. 31, no. 6, pp. 5115-5125, Nov, 2016.
- [19] H. Ahmadi, and H. Ghasemi, "Security-Constrained Unit Commitment With Linearized System Frequency Limit Constraints," *IEEE Transactions on Power Systems*, vol. 29, no. 4, pp. 1536-1545, Jul, 2014.
- [20] L. E. Sokoler, P. Vinter, R. Brentsen, K. Edlund, and J. B. Jorgensen, "Contingency-Constrained Unit Commitment in Meshed Isolated Power Systems," *IEEE Transactions on Power Systems*, vol. 31, no. 5, pp. 3516-3526, Sep, 2016.
- [21] J. F. Restrepo, and F. D. Galiana, "Unit commitment with primary frequency regulation constraints," *IEEE Transactions on Power Systems*, vol. 20, no. 4, pp. 1836-1842, Nov, 2005.
- [22] H. Chavez, R. Baldick, and S. Sharma, "Governor Rate-Constrained OPF for Primary Frequency Control Adequacy," *IEEE Transactions on Power Systems*, vol. 29, no. 3, pp. 1473-1480, 2014.
- [23] H. Saadat, *Power system analysis*: McGraw-Hill, 2009.

- [24] S. Chen, T. Lund, M. H. Zamastil, V. Akhmatov, H. Abildgaard, and B. C. Gellert, "Short-circuit calculations considering converter-controlled generation components" in IEEE Energytech, Cleveland, OH, USA, 2012.
- [25] DigSILENT PowerFactory. "Fault Current Calculation Complete Method in PowerFactory User's Manual," <https://www.digsilent.de/en/powerfactory.html>.
- [26] E.ON Netz GmbH. "E.ON Netz grid code high and extra high voltage," [http://www.pvupscale.org/IMG/pdf/D4\\_2\\_DE\\_annex\\_A-3\\_EON\\_HV\\_grid\\_connection\\_requirements\\_ENENARHS2006de.pdf](http://www.pvupscale.org/IMG/pdf/D4_2_DE_annex_A-3_EON_HV_grid_connection_requirements_ENENARHS2006de.pdf).
- [27] B. Weise, "Impact of K-factor and active current reduction during fault-ride-through of generating units connected via voltage-sourced converters on power system stability," *IET Renewable Power Generation*, vol. 9, no. 1, pp. 25-36, Jan. 2015.
- [28] Australian Energy Market Operator. "Electricity rule change proposal generator technical requirements," [https://www.aemo.com.au/-/media/Files/Electricity/NEM/Security\\_and\\_Reliability/Reports/2017/AEMO-GTR-RCP-110817.pdf](https://www.aemo.com.au/-/media/Files/Electricity/NEM/Security_and_Reliability/Reports/2017/AEMO-GTR-RCP-110817.pdf).
- [29] General Electric Energy, *Modeling of GE wind turbine-generators for grid studies*, General Electric International, Inc., 2010.
- [30] IEEE/NERC task force on short-circuit and system performance impact of inverter based generation, *Impact of inverter based generation on bulk power system dynamics and short-circuit performance*, 2018.
- [31] Manitoba HVDC Research Centre. "PSCAD cookbook synchronous machine studies," 2017; <https://hvdc.ca/knowledge-base/read/article/291/chapter-10-synchronous-machine/v>.
- [32] SIEMENS PTI. "Power system simulator for engineering (PSSE)," <https://www.siemens.com/global/en/home/products/energy/services/transition-distribution-smart-grid/consulting-and-planning/pss-software/pss-e.html>.
- [33] I. Kocar, J. S. Lacroix, and F. Therrien, "General and Simplified Computation of Fault Flow and Contribution of Distributed Sources in Unbalanced Distribution Networks," *IEEE Power and Energy Society General Meeting*, 2012.
- [34] Australian Energy Market Operator. "Transfer limit advice South Australia system strength for the national electricity market"; [https://www.aemo.com.au/-/media/Files/Electricity/NEM/Security\\_and\\_Reliability/Congestion-Information/2018/Transfer-Limit-Advice---South-Australian-System-Strength.pdf](https://www.aemo.com.au/-/media/Files/Electricity/NEM/Security_and_Reliability/Congestion-Information/2018/Transfer-Limit-Advice---South-Australian-System-Strength.pdf).
- [35] Australian Energy Market Operator. "Power system frequency and time deviation monitoring report – reference guide," 2019; [http://www.aemo.com.au/-/media/Files/PDF/Frequency\\_Report\\_Reference\\_Guide\\_v2\\_0.pdf](http://www.aemo.com.au/-/media/Files/PDF/Frequency_Report_Reference_Guide_v2_0.pdf).
- [36] F. Li, J. Kueck, T. Rizy, and T. King. "A preliminary analysis of the economics of using distributed energy as a source of reactive power supply," <http://info.ornl.gov/sites/publications/Files/Pub1771.pdf>.
- [37] DNV KEMA Energy & Sustainability. "System service provision an independent view on the likely costs incurred by potential system service providers in delivering additional and enhanced system services," <http://www.eirgridgroup.com/site-files/library/EirGrid/System-Service-Provision-DNV-KEMA-Report-2012.pdf>.
- [38] D. Rajan, and S. Takriti. "IBM RC23628 Minimum up/down polytopes of the unit commitment problem with start-up costs," 2018; [https://domino.research.ibm.com/library/cyberdig.nsf/papers/CDCB02A7C809D89E8525702300502AC0/\\$File/rc23628.pdf](https://domino.research.ibm.com/library/cyberdig.nsf/papers/CDCB02A7C809D89E8525702300502AC0/$File/rc23628.pdf).
- [39] C. M. Correa-Posada, G. Morales-Espana, P. Duenas, and P. Sanchez-Martin, "Dynamic ramping model including intraperiod ramp-rate changes in unit commitment," *IEEE Transactions on Sustainable Energy*, vol. 8, no. 1, pp. 43-50, Jan. 2017.
- [40] Gurobi Optimization. "Mixed-integer programming (MIP) – a primer on the basics," 2019; <https://www.gurobi.com/resource/mip-basics/>.
- [41] R. D. Zimmerman, C. E. Murillo-Sanchez, and R. J. Thomas, "MATPOWER: steady-state operations, planning, and analysis tools for power systems research and education," *IEEE Transactions on Power Systems*, vol. 26, no. 1, pp. 12-19, Feb. 2011.
- [42] M. Gibbard, and D. Vowles. "Simplified 14 generator model of the SE Australian power system," <http://www.eleceng.adelaide.edu.au/groups/PCON/PowerSystems/IEEE/BenchmarkData/index.html>.
- [43] Australian Energy Market Operator. "Australian Energy Market Operator interactive maps and dashboards," 2018; <http://www.aemo.com.au/aemo/apps/visualisations/map.html>.
- [44] NEM Review. "Australian national electricity market review," <http://www.nem-review.info/>.
- [45] Australian Energy Market Operator. "Interconnector capabilities for the national electricity market," 2018; [https://www.aemo.com.au/-/media/Files/Electricity/NEM/Security\\_and\\_Reliability/Congestion-Information/2017/Interconnector-Capabilities.pdf](https://www.aemo.com.au/-/media/Files/Electricity/NEM/Security_and_Reliability/Congestion-Information/2017/Interconnector-Capabilities.pdf).
- [46] "IEEE 9 bus system," <https://al-roomi.org/power-flow/9-bus-system>.
- [47] P. Kundur, N. J. Balu, and M. G. Lauby, *Power system stability and control*: McGraw-hill New York, 1994.



**Huajie Gu** (S'2016) received his B.Eng. degree in Automatic Control from Nanjing Technical University, Nanjing, China, in 2011, M.Eng. degree in Control Theory and Control Engineering from Tongji University, Shanghai, China, in 2014, and Ph.D. degree in Electrical Engineering from The University of Queensland, Brisbane, Australia, in 2019. He is currently working as a power system engineer at Australian Energy Market Operator, Brisbane, Australia. His research interests include renewable energy, generator dispatch and power system dynamic and transient analysis.



**Ruifeng Yan** (S'2009, M'2012) received the B. Eng. (Hons.) degree in Automation from University of Science and Technology, Beijing, China, in 2004, the M. Eng degree in Electrical Engineering from the Australian National University, Canberra, Australia, in 2007, and Ph.D. degree in Power and Energy Systems from the University of Queensland, Brisbane, Australia, in 2012. His research interests include power system operation and analysis, and renewable energy integration into power networks.



**Tapan Saha** (M'1993, SM'1997, F'2019) was born in Bangladesh in 1959 and immigrated to Australia in 1989. He received his B. Sc. Engineering (electrical and electronic) in 1982 from the Bangladesh University of Engineering & Technology, Dhaka, Bangladesh, M. Tech (electrical engineering) in 1985 from the Indian Institute of Technology, New Delhi, India and PhD in 1994 from the University of Queensland, Brisbane, Australia. Tapan is currently Professor of Electrical Engineering in the School of Information Technology and Electrical Engineering, University of Queensland, Australia. Previously he has had visiting appointments for a semester at both the Royal Institute of Technology (KTH), Stockholm, Sweden and at the University of Newcastle (Australia). He is a Fellow of the Institution of Engineers, Australia. His research interests include condition monitoring of electrical plants, power systems and power quality.



**Eduard Muljadi** (M'1982, SM'1994, F'2010) received his Ph.D. in electrical engineering from the Univ. of Wisconsin, Madison. He was a faculty at the California State University, Fresno (1988-1992). From 1992-2017, he worked at the National Renewable Energy Laboratory in Golden, CO. And, in January 2018, he joined Auburn University in Auburn, AL, as the James J. Danaher distinguished professor. His research interests include electric machines, power electronics, power systems, and renewable energy. He is a member of Eta Kappa Nu, Sigma Xi, a fellow of the IEEE, and an editor of the IEEE Transactions on Energy Conversion. He is member of various subcommittees within the IEEE Industry Application Society (IAS), Power Electronics Society, and Power and Energy Society (PES). He is the founding member and the past chair of Renewable Energy Machines and Systems subcommittee, and the chair of the Advanced Pumped Storage Hydropower Modeling Task Force within the PES. He holds patents in power conversion for renewable energy.